energies

MDPI

Article

Scale Effect on Hydraulic Properties of Pore-Fissure Deep Rock Formations and Its Importance for the Mining Shaft-Sinking Process

Maciej Pikuła [1], Krzysztof Chudy [2], Magdalena Worsa-Kozak [2,*] and Mariusz Czop [3]

[1] KGHM Cuprum Research and Development Centre, 53-659 Wrocław, Poland
[2] Faculty of Geoengineering, Mining and Geology, Wrocław University of Science and Technology, 50-421 Wrocław, Poland
[3] Faculty of Geology, Geophysics and Environmental Protection, AGH University of Science and Technology, 30-059 Kraków, Poland
* Correspondence: magdalena.worsa-kozak@pwr.edu.pl

Abstract: The problem of hydraulic parameters estimation lies in the depth: the deeper the rock formation, the more expensive and difficult the field tests and samples acquisition, and the more challenging the technical issues. The article assesses the Triassic sandstone's drainage potential at the stage of shaft sinking. It focuses on parameter analysis in varied scales, from drill-core sample laboratory testing, through a single well drawing test, to long-term pumping and recovery tests in the well with observation piezometers. The obtained results are compared to the values estimated in the past using different methods. Finally, the paper states whether it is reliable to forecast pore-fissure sandstone drainage potential based only on core samples' laboratory tests. This research proved that lab tests underestimate pore-fissure rocks' hydraulic parameters (mean hydraulic conductivity $k = 9.79 \times 10^{-8}$ m/s) tenfold more than long-term pumping tests (mean $k = 4.45 \times 10^{-7}$ m/s). However, it can be concluded that the group of so-called "witness samples", 10% of all core samples with a top value of the hydraulic conductivity tested in the laboratory, can be representative of the aquifer and comparable to the values obtained in pumping tests. With this in mind, we recommend using the highest values of hydrogeological parameters from laboratory tests based on the worst-case scenario. Therefore, it is possible to forecast inflows to the shafts reliably. This methodology is recommended only for rocks of porous and pore-fissure character.

Keywords: open porosity; specific yield; hydraulic conductivity; pumping test; Triassic sandstone

Citation: Pikuła, M.; Chudy, K.; Worsa-Kozak, M.; Czop, M. Scale Effect on Hydraulic Properties of Pore-Fissure Deep Rock Formations and Its Importance for the Mining Shaft-Sinking Process. *Energies* **2023**, *16*, 2263. https://doi.org/10.3390/en16052263

Academic Editors: Sergey Zhironkin and Dawid Szurgacz

Received: 9 December 2022
Revised: 8 February 2023
Accepted: 23 February 2023
Published: 27 February 2023

1. Introduction

The reliable hydraulic properties of pore-fissure rocks are crucial to the accurate prognosis of groundwater inflow to the sinking shafts. Moreover, they determine the safety of mining operations and water management strategies. For example, a known unpredicted catastrophic influx to the sinking shaft is the R-XI shaft accessing Poland's "Rudna" copper ore deposit [1]. Groundwater intrusion in 2002/2003 stopped the sinking process at a depth of 600–635 m for nearly a year and showed that more attention must be paid to hydrogeology when accessing deep deposits. Copper ore deposits in Poland's Fore-Sudetic Monocline (FSM) have been exploited for more than 60 years. As a result of many years of mining, the resource base decreases, making it necessary to mine in deeper and less accessible parts of the copper ore body. However, access to mineral resources at greater depths is performed within complicated geological and hydrogeological conditions, causing health and safety challenges. Appropriate solutions for the ore body-opening technology should be based on reliable geological and hydrogeological research results. The best method of assessing these conditions should rely on a factual assessment of the previous exploration methods. Combined with an analysis of the predicted and measured data,

weaknesses, and strengths of particular practices have been indicated. Hydrogeological research preceding the design and construction of a shaft, if performed on a limited scale or using low accuracy and reliability methods, provides incomplete and unreliable data [2]. Such imprecise recognition of hydrogeological conditions and geological structure leads to inaccurately estimated inflows, as was proved during the long-term exploitation in FSM (Figure 1). As a result, several critical influxes occured during shafts' sinking and disrupted or even stopped the process [1,3–5].

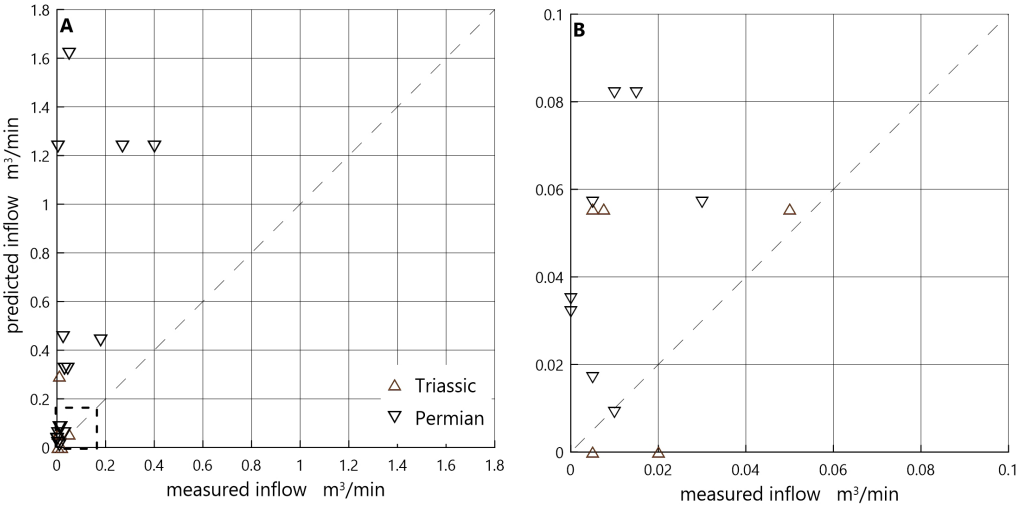

Figure 1. Comparison of predicted and measured inflows into the sinking shaft R-XI; (**A**) complete data, (**B**) data in the range up to 0.1 m^3/min (black square in (**A**); [2] modified).

The problem of adequately identifying hydrogeological conditions in the copper mining area in FSM began to be described in the 1970s and 1980s [3,6,7] and remains valid. It became more important with the development of numerical modeling methods and their implementation to prognoses of water inflow to underground mine workings [2,5,8,9]. However, the software development was not followed by the explicit recognition of rock mass filtration parameters. As a result, it caused problems in properly defining boundary conditions or hydrogeological schematization [10] and adequate integration of laboratory and field measurements [11,12]. Similar challenges were noticed in hydrogeological modeling in mining areas worldwide. For example, one of the first review papers on data reliability and quality and the investigation methodology for determining the hydraulic parameters necessary for the initial inflow to shafts estimations for modeling purposes highlighted the importance of field tests in drill holes [13]. Likewise, the application of groundwater flow modeling for mining purposes and data quantity and quality challenges were widely described based on examples from the Czech Republic [14]. However, predictions of groundwater states and flows based on numerical modeling are challenging in mining and every application. Accurate recognition of hydrogeological parameters of rock mass for shaft-sinking purposes is also crucial for proper design of the sinking technology [15,16]. Thus, special attention must be paid to data collection, which was presented in detail based on the case study of the Death Valley regional groundwater flow system [17]. Cases from Poland and other countries mentioned above show that more attention must be paid to the hydrogeological properties of individual water-bearing horizons. For deep multilayered aquifers, it is a considerable challenge mining engineering, hydraulic engineering, and hydrogeology must face minimizing the risk of disaster, specifically at the stage of shafts sinking.

The accuracy and reliability of estimated hydrogeological parameters of rocks and soils vary with the scale of the investigation [18–24]. In most cases, the lowest values are obtained on the test in the smallest point scale, such as laboratory tests of soil or core samples [18,21,23]. In contrast, the largest values that characterize rock mass on a local or

regional scale are derived by the filed tests (single- or cross-borehole pumping tests) [19–21]. The novelty presented by our work is comparing different methods of hydraulic properties' estimation and an indication of the most reliable methodology of their evaluating for shaft sinking in the pore-fissure rocks.

Our study provides: (1) reliable and unique data on Triassic pore-fissure sandstone parameters as a referential for numerical modeling, (2) best practice guidance on the usefulness of the results obtained in different scales, (3) hydrogeological parameters of the Middle and Lower Bunter sandstone in FSM are the objectives of this study. It has been done based on field and laboratory tests presented in this article and allowed for comprehensive hydrogeological characteristics of sandstone formations, classified as the Middle and Lower Bunter sandstone, together with an assessment of their drainage potential at the stage of shaft construction. Moreover, we ask whether it is reliable to forecast pore-fissure sandstone drainage potential based only on core samples' laboratory tests. We answer this question by analyzing porosity, specific yield, storage coefficient, and hydraulic conductivity, examined in varied scales from drill-core samples' laboratory testing and a single well-drawing test to long-term pumping and recovery tests in the cross-borehole. The novel approach was implemented based on the methodology for estimating representative values of hydrogeological parameters for pore-fissure rocks, taking into account the often overlooked laboratory tests for samples derived from drill cores. Finally, the obtained results are compared to the values estimated in the past using different methods and matched with real inflows.

2. Materials and Methods

2.1. Study Area

The study area is situated in southwestern Poland on the FSM, between Gawronki and Gawrony (Figure 2) in the north-eastern part of the Retków copper ore deposit, which is a prospective part deposit designated for future exploitation.

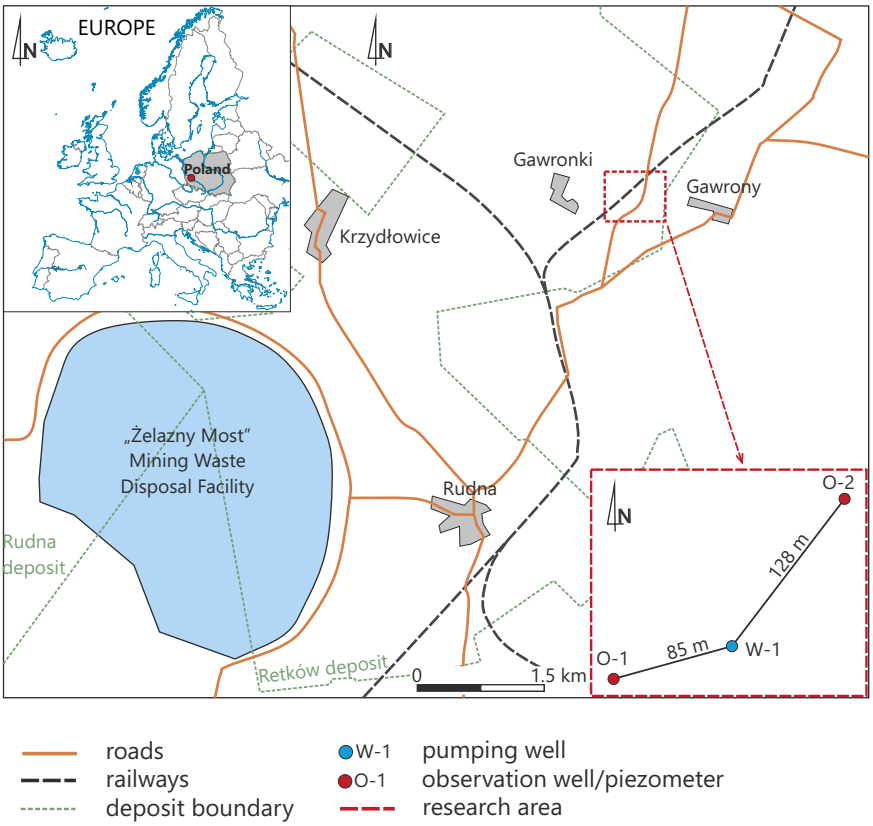

Figure 2. Location of the research area within a copper ore deposit.

The bedrock of the FSM is a complex of crystalline rocks formed in the Proterozoic and older Palaeozoic periods (Figure 3) [25]. The Permian formations are represented by the Rotliegendes sediments of red-colored conglomerate, shale, sandstone, and higher volcanic rocks (rhyolite, rhyolitic tuff) [26]. They are overlaid by brownish-red sandstone, which changes into grey and white in the upper part. Zechstein sediments are copper-bearing shale, limestone, dolomite, anhydrite, rock salt, and clay shale [27], and overlay the Rotliegendes part. The Zechstein is divided into four cyclothems: Aller (Z4), Leine (Z3), Stassfurt (Z2), and Werra (Z1) (Figure 3). Triassic deposits, represented by the lower and middle Triassic, lie conformably on the Zechstein formations. In the L=lower Triassic, the Bunter sandstone is represented by sandstone, siltstone, and shale with limestone interbeds in the lower and middle parts. The upper part of the lower Triassic (Röt Formation) is characterized by marl, shale, siltstone, dolomite, limestone, anhydrite, and gypsum with interbeds of marl. The Middle Triassic, represented by Muschelkalk, comprises limestone, dolomite, marl, anhydrite, and gypsum. The Cenozoic formations are characterized by Paleogene, Neogene, and Quaternary formations, which lie unconformably on Triassic deposits. The Palaeogene–Neogene sediments are mainly quartz sand, glauconitic sand, and clay with an interbedding of mud or sand. Quaternary formations consist of sand, gravel, clay, and silt of the Southern and Central Poland glaciations. The Quaternary is characterized by high lithological variability in vertical and horizontal profiles.

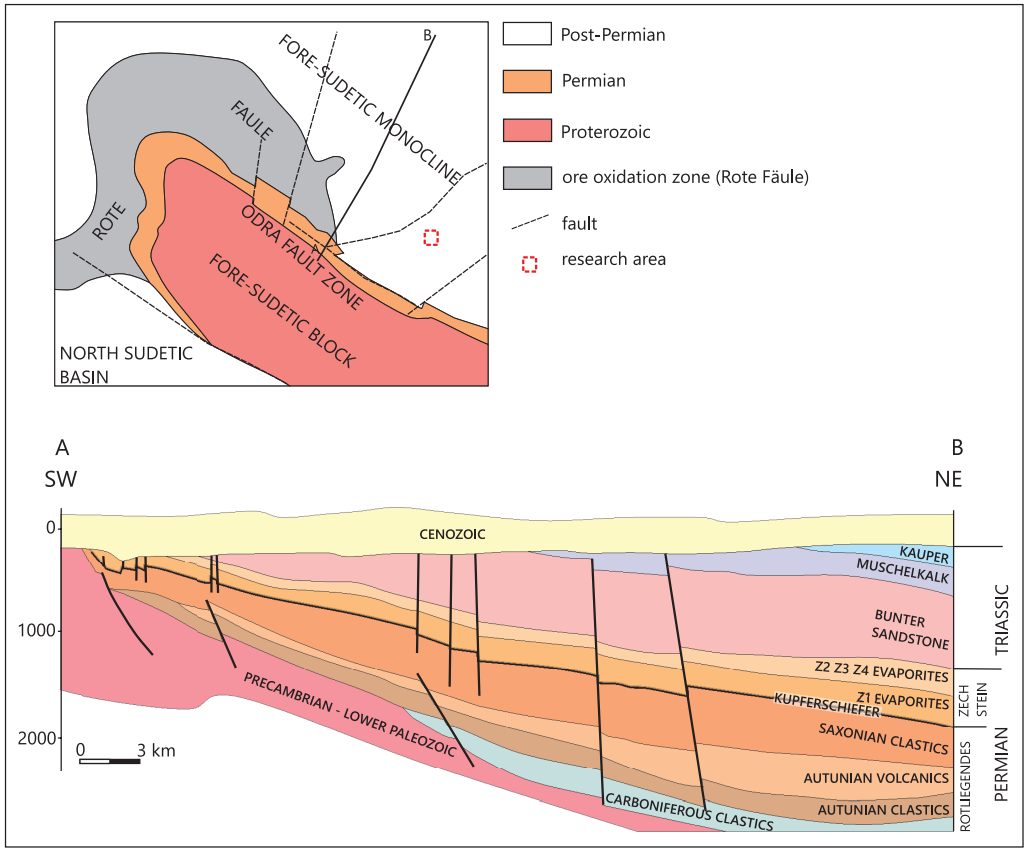

Figure 3. Location and geologic setting of the research area. Geologic cross-section along line A–B in upper figure [28].

The hydrogeologic profile of the study area includes four aquifers: Quaternary, Neogene–Paleogene, Triassic, and Permian (Figure 4) [5]. The Quaternary aquifer covers sandy and sandy-gravel water-bearing layers of the Holocene and Pleistocene, which are usually separated from lower layers by Pliocene clays of the Poznan series.

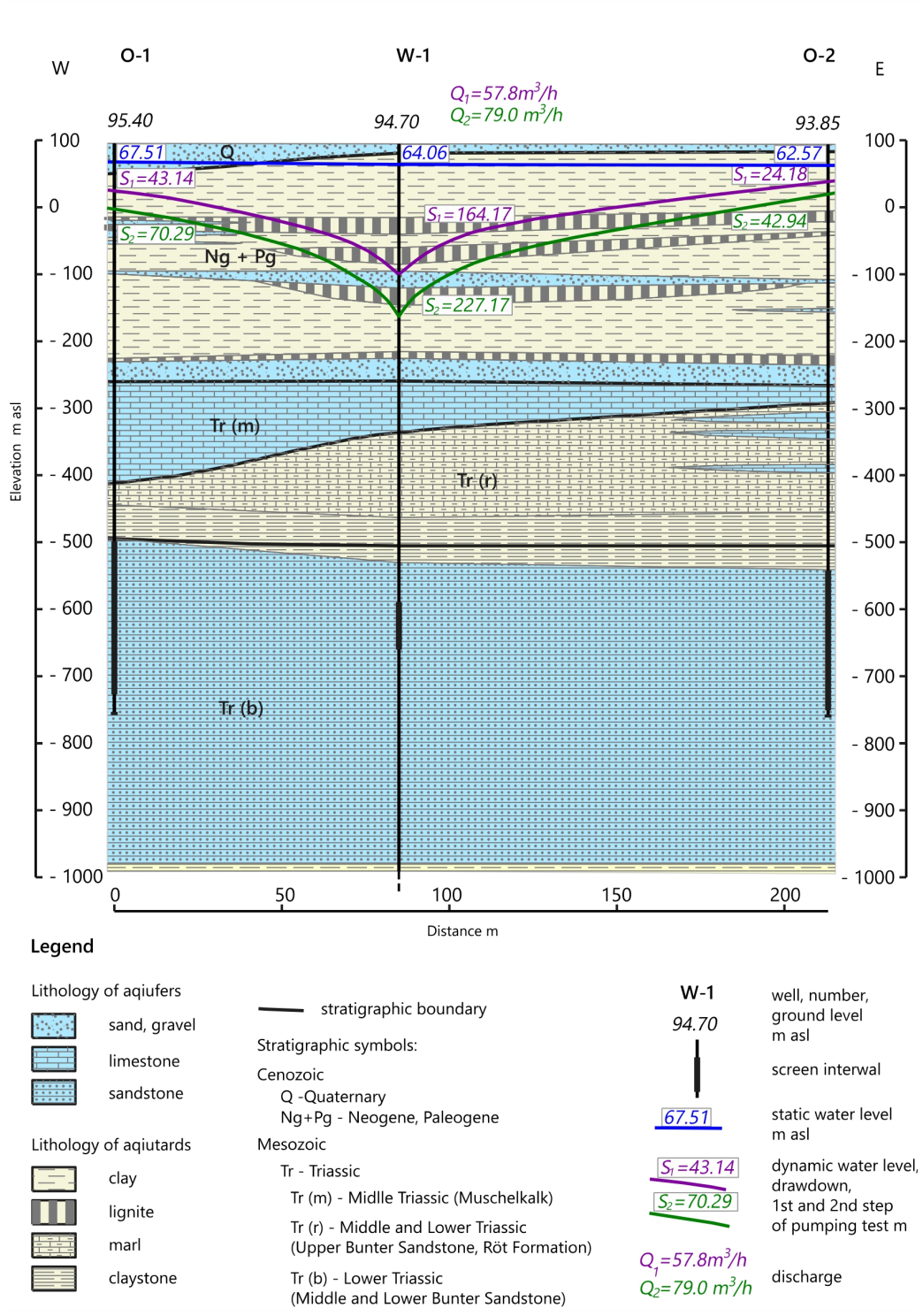

Figure 4. Scheme of hydrogeological conditions of the pumping test area.

The Neogene–Paleogene water-bearing horizon includes water in sandy and sandy-gravel layers within isolating layers: clay, silt, and brown coal. Three water-bearing horizons can be distinguished within this horizon: over-coal (Pliocene and upper Miocene), inter-coal (middle and lower Miocene), and under-coal (Oligocene). These three levels of the Neogene–Pliocene aquifer may have hydraulic connectivity locally. The subject of the presented research, the Triassic aquifer, is distinguished by an aquifer of shell limestone, upper Bunter sandstone (Röt Formation), and middle and lower Bunter sandstone. The middle and lower Bunter sandstone aquifer's water occurs in the arkose sandstone, more

rarely in quartz sandstone. This sandstone is interlayered with insets of poorly permeable and impermeable sediments—shale and gypsum. The studied sandstone is characterized by diversified grain sizes—from fine- to coarse-grained. Water-bearing formations of the discussed zone occur in most of the FSM area. Sub-Cenozoic outcrops of this aquifer in the area of the monocline spread in a wide belt, several kilometers wide, located to the northeast of outcrops of older, lower Zechstein formations (cyclothem Z4). Paleogene sediments are present above the sub-Cenozoic outcrops of this aquifer in unconsolidated sandy formations and isolating layers of silt and clay. To the north and north-west of the sub-Cenozoic outcrops of the middle and lower sharp sandstone, the aquifer is covered by isolating sediments (mudstones) overlain by carbonate water-bearing sediments of the upper Bunter sandstone and Muschelkalk. The middle and Bunter sandstone sediments are underlaid by separating rocks of Zechstein's siltstone and anhydrite. In the copper-bearing area, the thickness of the Middle and Lower Bunter sandstone completely disappears in the southwestern region of its sub-Cenozoic outcrops. In the northern areas of the documented copper ore deposits, the maximum thickness reaches approx. 600 m. In the study area, the thickness of sediments of this aquifer ranges about 450 m. The hydraulic conductivity of the discussed aquifer in the copper-bearing area of the FSM ranges between 10^{-9} m/s ÷ 10^{-6} m/s [29]. The Permian aquifer comprises the Zechstein and Rotliegendes aquifers and includes sedimentary and relict water. It is built of dolomite, limestone, and gray and red sandstone separated by impermeable layers.

2.2. Methods and Calculations

2.2.1. Field Test

Field hydrogeologic investigations in the middle and lower Bunter Sandstone aquifer were based on pumping tests in the well (W-1) with two observation wells (O-1, O-2; Figure 2). The pumping test ran between 08.07 and 02.09.2016 at a depth from 684.7 m to 755.0 m. It covered purge pumping and measurement pumping. Each was completed by recovery of the water level. Purge pumping was conducted to remove the drilling mud and decontaminate the near-borehole zone [30,31]. A submersible electronic hydrostatic pressure sensor—APLISENS SG-25, and a backup Solinst Levelogger Edge water level sensor were used for constant, automated observation of the water level in the wells. Additionally, control manual measurements were taken with the SEBA Electric Contact Meter Type KLL. The pumping test flow rate was measured using an electromagnetic flow sensor Siemens MAG 3100. The pumping test was performed as a two-drawdown step procedure (Figure 5) [30]. The first drawdown step was carried out with the pumping rate of 60.0 m^3/h for 9 days and 23 h, and the second was carried out with the rate of 80.0 m^3/h for 40 days and 1 h 30 min. After the pumping test was completed, observations of water table recovery in the boreholes were conducted for 74 days in the pumping borehole and 56 days in the piezometers. Interpreting the pumping test with the determination of the hydraulic conductivity was carried out using methods for non-steady flow. The hydraulic conductivity and storage coefficient was determined based on measurements from a pumping borehole (W-1) and two piezometers (O-1 and O-2) using the AquiferTest software. For the W-1 borehole, both for the period of pumping and stabilization of the water table, methods were applied which consider the influence of so-called "well effects" on the obtained measurement results. For measurements from pumping, "Agarwal's method" was used, and for measurements from stabilization, "Agarwal's solution" was applied, taking into account the assumptions of the above method [32–34]. Measurement data from piezometers O-1 and O-2 were interpreted using the Theis method, and for data from the stabilization period, the Theis method, Agarwal's solution [32,34,35]. Data from the complete pumping and stabilization period were included in the interpretation. Only the initial 10 min of the 2nd pumping step were omitted because of the significant stepwise variability in the magnitude of the pumping rate. For the 1st and 2nd pumping test steps, the variability in pumping rates during the tests was included in the calculations.

For comparison of parameters estimated with the software storage coefficient was also calculated using the formula [36]:

$$S = 3 \times 10^{-6} b \quad (1)$$

where b is saturated aquifer thickness in meters.

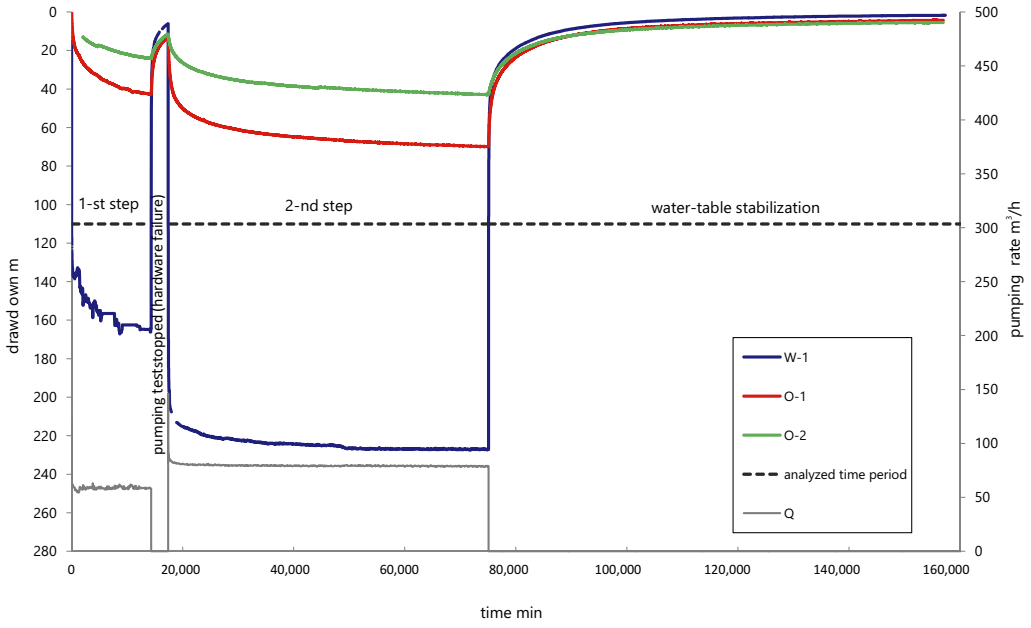

Figure 5. Pumping test progress.

The rock quality designation (RQD) index, developed by Deere et al. (1967) [37], was also implemented to analyze hydrogeological parameters. RQD is defined as the borehole core recovery percentage or ratio incorporating only pieces of a solid core longer than 100 mm in length measured along the core's centerline of the core [38]. It is distinguished for selected structural domains or specific sizes of core [39]. It was estimated in the field while the core was logged during the drilling operations.

2.2.2. Laboratory Test

Laboratory studies were also significant in determining aquifer parameters. After the drilling of boreholes, rock samples were taken from drill cores to test hydrogeological parameters in terms of open porosity (p_o), specific yield (S_y), and hydraulic conductivity (k). The hydrogeological parameters of sandstone were studied on 36 samples at the AGH University of Science and Technology in Krakow. Samples were taken from those sections of the core that allowed a smaller diameter sample to be cut. The samples ready to test were cylindrical (diameter 50 mm; length 55 mm, (Figure 6A)). First, the open porosity was determined. The next step was the determination of specific yield using a high-speed centrifuge. Finally, hydraulic conductivity was determined.

Open porosity *(p_o)* (interconnected porosity) is one of the elementary microstructural characteristics of rocks. It determines the proportion of interconnected pores regardless of their size in the volume of the rock sample. Tests were performed based on the method described in the literature and saturating samples in water, called the Archimedes' method [10,40–43]. The value of the open porosity was calculated from the formula [43,44]:

$$p_o = (G_a - G_d)/(G_a - G_w) \times 100\% \quad (2)$$

where G_a is the weight of the sample saturated with water (24 h) and weighed in air, G_d is the weight of the sample dried at 110 °C for 24 h, G_w is the weight of the sample saturated with water (24 h) and weighed in water.

To determine the ability of rocks to drain free water under the effect of gravity, we estimated the specific yield (S_y), which defines the volume of water that can drain away from a unit volume of rock [36,45,46]. The method used to determine the rock's S_y is based on a laboratory centrifuge (Figure 6B) [47,48].

Figure 6. Core prepared for parameter determination (**A**), samples placed in a high-speed centrifuge (**B**), test equipment for measurement of k (**C**).

The centrifuge's speed is adjusted to the height of the sample to simulate a negative pressure of 10 m of the water column, which is assumed to be the maximum value occurring in nature and simulates natural drainage lasting 5–20 years. This value is used in international research [10,42–44,49]. The S_y was calculated from the formula:

$$S_y = V_w / V_r \quad (3)$$

where V_w is the volume of drained water released by a suction pressure equivalent to a water column 10 m high (cm^3), V_r is the volume of the sample/rock (cm^3).

All the samples were centrifuged for 30 min, equivalent to the percolation time under natural conditions from 2 to 2.5 years. This interval was calculated according to Prill et al. [48] as the relationship between percolation time (T_n) of gravitational water in nature and centrifugation time (t):

$$(T_n / t) = (a / g)^2 \quad (4)$$

where: a—centrifugal acceleration, g—gravity.

Hydraulic conductivity (k) is one of the most important parameters used in hydrogeology. It is determined from the measured intrinsic permeability (k_p). Intrinsic permeability was determined in Dulinski's [50] apparatus, the gas permeameter (Figure 6C). This works on forcing the flow of compressed gas (liquid) through the dried sample. The

absolute pressure "before" and "after" the sample and the amount of gas flow is measured. Formula (5) [42,43] is used for calculations:

$$k_p = 2Qpl\eta / F(p_1^2 - p_2^2) \quad (5)$$

where: k_p is intrinsic permeability (Darcy), Q is the volume of flowing gas (cm^3/s), p is atmospheric pressure (at), l is sample length (cm), η is dynamic gas viscosity coefficient (cP), F is sample cross-sectional area (cm^2), p_1 is the pressure of gas before sample (at), p_2 is the pressure of gas behind sample (at).

The Formula (6) describes the relationship between intrinsic permeability and hydraulic conductivity [43]:

$$k = k_p(\gamma_w / \eta_w) \quad (6)$$

where: k—hydraulic conductivity (cm/s), k_p—intrinsic permeability (Darcy), γ_w—water specific gravity (g/cm^3), η_w—water dynamic viscosity coefficient (cP).

From (6) we find that (at temp = 10 °C):

$$k = 7.66 \times 10^{-6} k_p \quad (7)$$

3. Results

3.1. Field Test

The value of hydraulic conductivity k determined on measurements from the first step of test pumping for the W-1 borehole was 3.31×10^{-7} m/s. For the observation wells, it was 3.71×10^{-7} m/s (O-1) and 5.80×10^{-7} m/s (O-2). The arithmetic mean of the whole system (pumping well with observation wells) was 4.27×10^{-7} m/s.

Based on measurement data obtained in the second step of the pumping test, the calculated value of k for the test borehole (W-1) was 3.82×10^{-7} m/s, and for the observation wells—3.92×10^{-7} m/s (O-1) and 5.62×10^{-7} m/s (O-2). As a result, the arithmetic mean value of the k equal 4.45×10^{-7} m/s was calculated for the whole system (pumping well with observation wells) (Figures 7–10).

Measurements made during water table recovery in a pumping well (W-1; (Figure 11) determined k of 3.88×10^{-7} m/s and in observation wells—3.71×10^{-7} m/s (O-1) and 4.58×10^{-7} m/s (O-2) (Figure 12), on average for the whole system (pumping well with observation wells)—4.06×10^{-7} m/s.

Matching calculated depression with measured depression (Figure 13), as well as matching statistics (Table 1), indicate that the above parameters calculations are reliable.

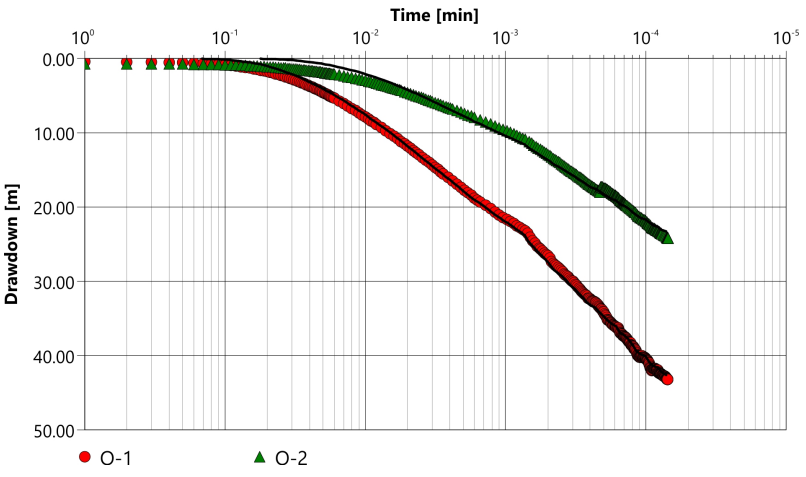

Figure 7. Analytical diagram for measurements in O-1 and O-2 during the first step of the pumping test (Theis method).

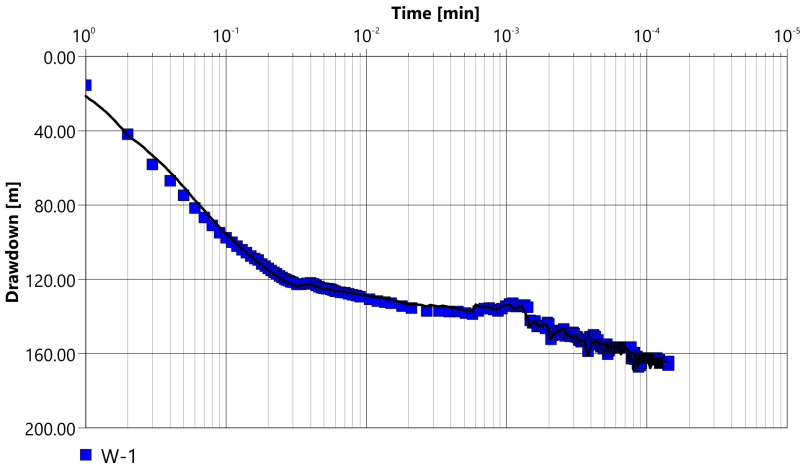

Figure 8. Analytical diagram for measurements in W-1 well during the first step of the pumping test (Agarwal's method).

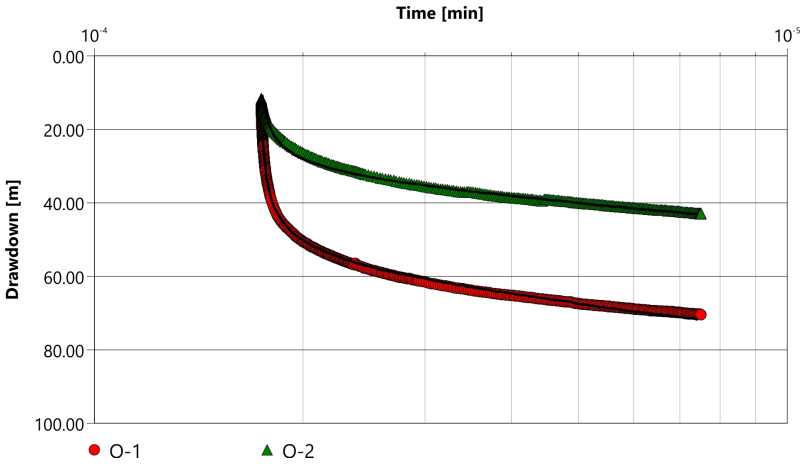

Figure 9. Analytical diagram for measurements in O-1 and O-2 during the second steps of the pumping test (Theis method).

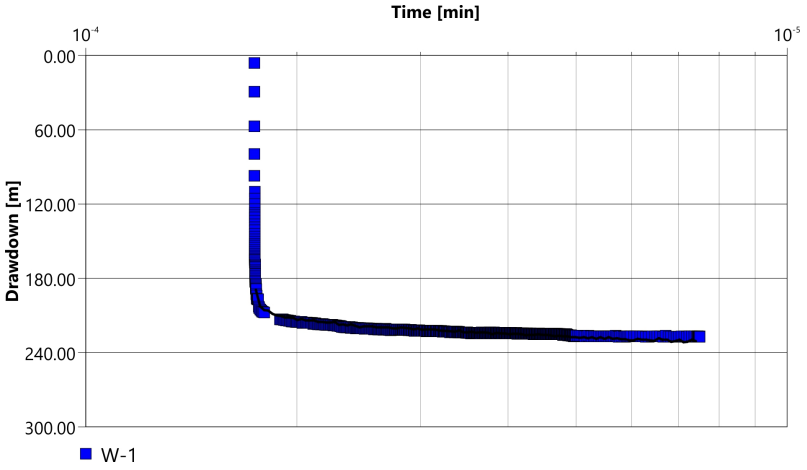

Figure 10. Analytical diagram for measurements in W-1 well during the second step of the pumping test (Agarwal's method).

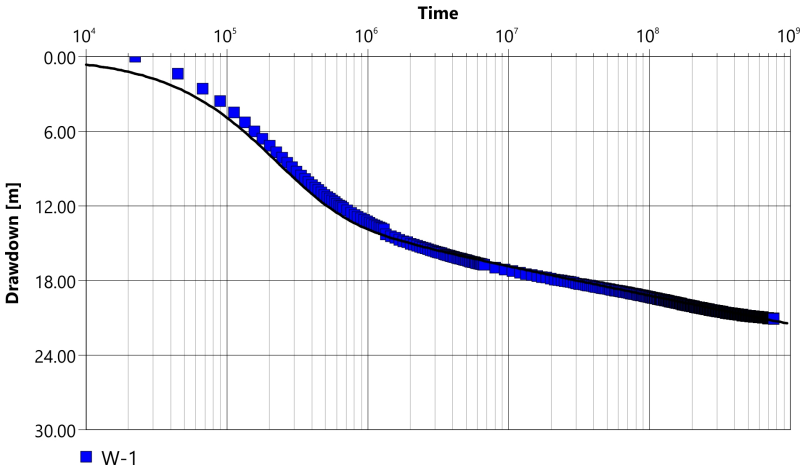

Figure 11. Analytical diagram for measurements during recovery in the W-1 well (Agarwal's method considering well effects + Agarwal's solution).

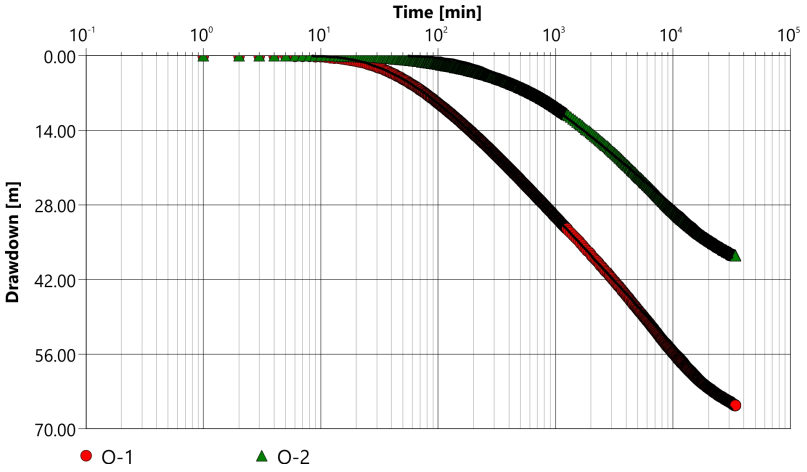

Figure 12. Analytical diagram for measurements during recovery in observation wells O-1 and O-2 (Theis method + Agarwal's solution).

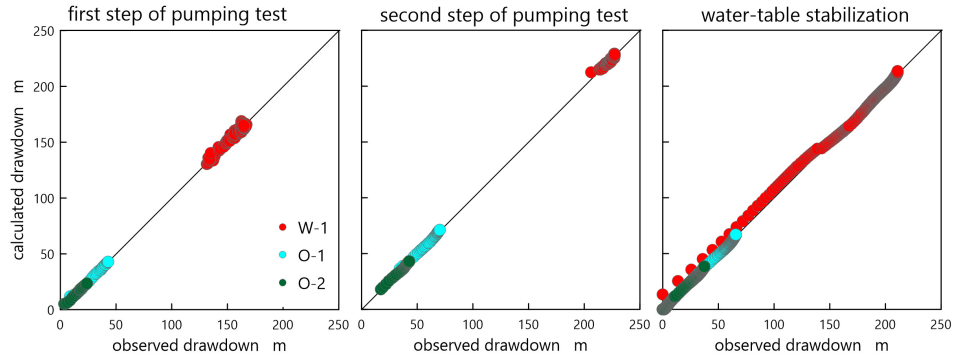

Figure 13. The plot of measured borehole depression vs. value calculated by the software

The results obtained from the pumping test classify the rocks into semi-permeable [51] or low-permeable rocks [52]. The water storage coefficient *S* value was also determined based on the analyses performed. Averaged values of this parameter for observation wells O-1 and O-2 of the first and second step of the pumping test are equal to 2.27×10^{-4} and 2.18×10^{-4}, respectively, and the average value for measurements during recovery is 4.02×10^{-4}. A similar result, 4.49×10^{-4}, was obtained from Formula (1) calculations by which the *S*-value is estimated from the thickness of the aquifer.

Table 1. Matching statistics between measurements taken during the pumping test and model values calculated with the software.

Pumping Test	Well No	Mean Δs [m]	Sum of Squared Errors [m^2]	Variance [m^2]	Standard Deviation [m]
1st step	W-1	0.014	799.087	3.386	1.84
1st step	O-1	0.054	59.743	0.234	0.484
1st step	O-2	0.108	42.545	0.212	0.460
2nd step	W-1	0.003	795.837	0.846	0.920
2nd step	O-1	0.007	173.542	0.496	0.704
2nd step	O-2	0.014	81.773	0.224	0.473
Recovery after 2nd step	W-1	−0.097	4578.936	3.134	1.770
Recovery after 2nd step	O-1	−0.003	1367.277	0.522	0.722
Recovery after 2nd step	O-2	0.074	1038.755	0.396	0.630

3.2. Laboratory Test

3.2.1. Characteristics of the Rock Samples

Macroscopic analysis of the rock samples identified three groups of sandstone: very fine-grained, fine-grained, and medium-grained.

The very fine-grained sandstone samples (seven samples) occur in the depth interval of 604–687 m in single layers of small thickness. These are samples of red or brownish-red quartz sandstone with gray layers added. They are layered flat-parallel or have wavy lamination. The mineral composition is dominated by transparent and semitransparent quartz grains, mainly pink, of spherical or ellipsoidal shape. The shape of the grains is semi-sharp to rounded. The lithic components are light and dark micas. Ferrosilicate binder predominates.

Fine-grained sandstone was the most popular in the analyzed samples and occurred in the complete profile (24 samples) as red or brownish-red quartz sandstone. In the depth interval of 640.0–644.0 m and 697.0–730.0 m, light gray and light green color dominates. Flat-parallel lamination up to 1mm thick predominates. Quartz dominates the mineral composition with semitransparent, pink, or grey grains. Grains are spherical and semi-rounded to rounded. The lithic constituents are light and dark micas. Silica binder predominates.

Medium-grained sandstone represents the minor group of four analyzed samples. They occur locally below 700.0 m and comprise red-brown to reddish quartz sandstone. Flat-parallel, continuous lamination dominates here, and laminae are light red and brownish red. The main mineral component is transparent and semitransparent Quartz, locally pink or yellow. Grains are semi-rounded and shaped spherical or ellipsoidal. The lithic components are light and dark micas and clay minerals. The sandstone is brittle and porous. Iron–silica or clay–silica binder dominates.

3.2.2. Interconnected Porosity (p_o)

The studied sandstone's open porosity (p_o) is relatively high. Values are between 0.0098 (Table 2) and 0.1894, with a mean of 0.0918 and a standard deviation of 0.0105. Very fine-grained and fine-grained sandstone showed similar p_o values. However, the highest p_o values were recorded for medium-grained sandstone (mean 0.1308).

The distribution of p_o is not homogeneous. Two subgroups with a similar parameter distribution can be distinguished but shifted to each other (Figure 14). In the first subgroup, we have fine-grained sandstone with low p_o (up to about 0.06). Sandstone with much higher p_o values (0.12–0.19) is placed in the second subgroup. Lower values belong to fine-grained sandstone ($p_o < 0.15$), and higher $p_o > 0.15$ to very fine-grained and medium-grained sandstone.

Table 2. Statistics of the measurement date set.

Rock Type	Parameter	Very Fine-Grained Sandstone	Fine-Grained Sandstone	Medium-Grained Sandstone	Sandstone in Total
p_o	Number of samples	6	24	4	34
	Min.	0.0098	0.0136	0.0614	0.0098
	Max.	0.1893	0.1829	0.1820	0.1894
	Arithmetic Mean	0.0807	0.0881	0.1308	0.0918
	Geometric Mean	0.0514	0.0219	0.1211	0.0683
	Median	0.0401	0.0583	0.1398	0.0624
	Standard Deviation	0.0771	0.0583	0.0521	0.0611
	Variance	0.0059	0.0034	0.0027	0.0037
S_y	Number of samples	1	13	3	17
	Min.	-	0.0017	0.0160	0.0018
	Max.	-	0.0849	0.0495	0.1059
	Arithmetic Mean	-	0.0422	0.0374	0.0451
	Geometric Mean	-	0.0219	0.0333	0.0259
	Median	-	0.0389	0.0466	0.0466
	Standard Deviation	-	0.0322	0.0185	0.0327
	Variance	-	0.0010	0.0003	0.0011
k	Number of samples	5	23	3	31
	Min.	7.00×10^{-12}	4.25×10^{-12}	3.67×10^{-10}	4.25×10^{-12}
	Max.	1.65×10^{-6}	4.89×10^{-7}	1.85×10^{-7}	1.65×10^{-6}
	Arithmetic Mean	3.31×10^{-7}	5.10×10^{-8}	6.90×10^{-8}	9.79×10^{-8}
	Geometric Mean	1.22×10^{-10}	4.58×10^{-10}	1.22×10^{-10}	5.24×10^{-10}
	Median	9.73×10^{-12}	5.31×10^{-10}	2.17×10^{-8}	3.67×10^{-10}
	Standard Deviation	7.40×10^{-7}	1.14×10^{-7}	1.01×10^{-7}	3.06×10^{-7}
	Variance	5.47×10^{-13}	1.29×10^{-14}	1.02×10^{-14}	9.39×10^{-14}

3.2.3. Specific Yield (S_y)

S_y values were measured for 17 samples of fine-grained sandstone. The remaining 17 samples were mechanically disintegrated at the centrifugation stage. Unfortunately, this does not allow a comparison of results for the three distinguished sandstone groups. The S_y value of tested samples ranges from 0.0018 to 0.1059 (Table 2). The arithmetic mean is 0.0451, with a standard deviation of 0.0079.

3.2.4. Hydraulic Conductivity (k)

The last measured parameter in the laboratory tests was the hydraulic conductivity (k), determined for 31 samples. Measurements were made three times, and the average of these three measurements was taken for analysis. The k of the sandstone matrix shows variation from 4.25×10^{-12} m/s to 1.65×10^{-6} m/s; the geometric mean is 9.79×10^{-8} m/s, and the standard deviation is 3.06×10^{-7} m/s. Very fine-grained and fine-grained sandstone show very similar k values (Table 2). In medium-grained sandstone, the lower limit of the k value is two orders higher than in fine-grained.

The distribution of k values is logarithmic but not homogeneous (Figure 14). Three subgroups can be distinguished. The first is sandstone with a very low k value (7.37×10^{-12} m/s to 9.73×10^{-12} m/s), mainly fine-grained and very fine-grained, probably with small pore sizes. The second subgroup is very fine-grained, fine-grained, and medium-grained sandstone with k oscillating between 1.58×10^{-11} m/s to 1.39×10^{-9} m/s). In this case, the slope of the approximating line is significantly lower, which indicates a more significant variation

in the pore space distribution in the samples. The third group consists of sandstone with higher permeability values (1.26×10^{-8} m/s to 1.65×10^{-6} m/s)) and well-developed pores where individual pores connect and enable water flow. The macroscopic observations show that the samples with clay interlayers tended to have lower k values than those without clay interlayers.

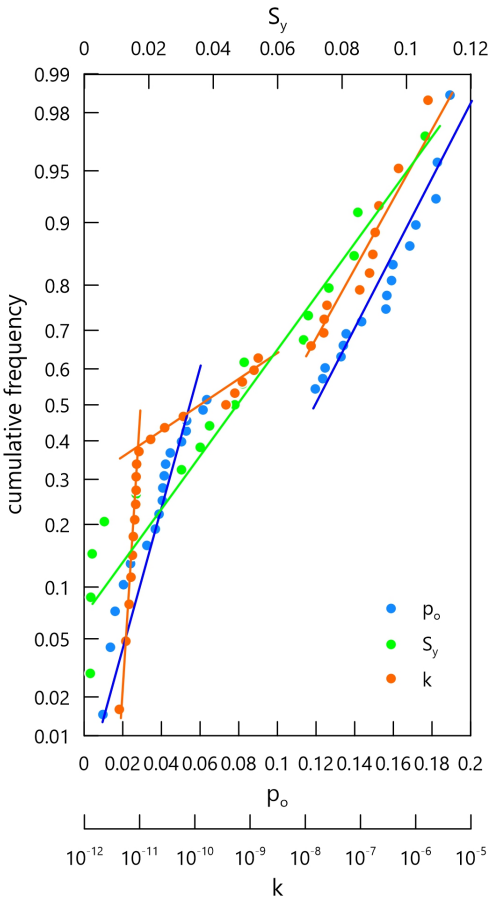

Figure 14. Cumulative frequencies of p_o, S_y, and k [m/s].

3.2.5. Variation of the RQD and Hydrogeological Properties with Depth

The analysis of changes in the described parameters should start with assessing the quality (strength) of the drill core since it describes the mechanical strength of rocks and indirectly tells about the binder that holds grains together. The RQD index was used for this purpose, and its analysis indicates that the studied rock mass has different mechanical strengths depending on the depth (Figure 15). Three zones with different RQD values can be distinguished. The first zone begins at 595.0 m and extends to a depth of 723 m. In this zone, the rock mass shows high mechanical strength, RQD > 80 for most of this zone (Figure 15). The exception is the interval from the depth of 690.0 m to 700.0 m, where locally, the RQD drops to the value of 60–63. Below the depth of 730 m, the zone of weakened rock mass begins, where the RQD index drastically drops to the value from 20 to 50. In an interval of 735–737.5 m, it reaches a minimum value of RQD = 0, and at a depth between 747.0 and 750.2 m, RQD equals 6.25. This zone ends at a depth of 796.0 m, where there is a significant increase in the strength of the rock mass RQD > 80, with local zones of weakness in the range of 804.0 m–808.0 m and 810.0 m–814.0 m. Such a distribution of RQD indicates the mechanical strength of the rock mass translated into the ability to collect samples for laboratory testing. Therefore, samples were taken from those strong enough fragments to be mechanically processed (cutting smaller core fragments of a specific, smaller diameter). In addition, the samples had to have sufficient mechanical strength to survive centrifugation in a high-speed centrifuge. For this reason, there are no samples from core fragments with

RQD < 50. There is no evident variability of hydrogeological parameters with depth. It is possible to distinguish zones in the profile with low values interspersed with zones with high values of measured parameters. The zones with low values are the depth zones 625.0 m–640.0 m, 680.0 m–700.0 m, and below 810 m (Figure 15). A slight correlation between their occurrence with local zones of reduced RQD can be noticed.

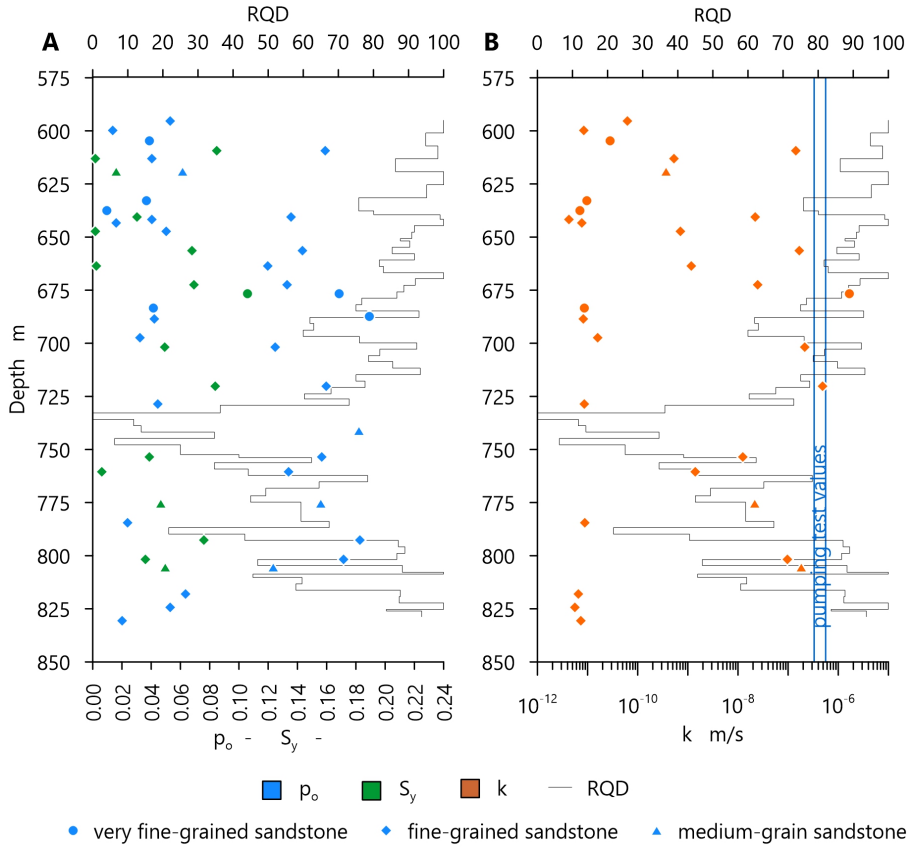

Figure 15. Distribution of p_o, S_y (**A**) and k (**B**) in the vertical profile.

3.2.6. Correlation between Hydrogeological Parameters

The arrangement and geometry of the matrix determine the values of p_o, S_y, and k. The homogeneity of the grain size, the shape of the grains, and the degree of grain cementation influence this. The degree of grain cementation will be indirectly indicated by the RQD parameter, the variation of which with depth was discussed earlier. The correlation between RQD and depth is moderately negative. Negative moderate correlation between RQD and p_o is evident (Figure 16, Table 3).

The analysis shows a fairly strong correlation between p_o and S_y (R = 0.70) (Figure 17). Correlation analysis for k shows its moderate correlation with S_y (R = 0.67) and p_o (R = 0.45). On the other hand, there is no visible correlation between depth and S_y and k, as well as between RQD and S_y and k.

Table 3. Correlation matrix between measured parameters.

	Depth	p_o	S_y	k	**RQD**
depth	1.00	0.27	0.13	0.00	−0.62
p_o	0.27	1.00	0.70	0.45	−0.49
S_y	0.13	0.70	1.00	0.67	−0.08
k	0.00	0.45	0.67	1.00	−0.03
RQD	−0.62	−0.49	−0.08	−0.03	1.00

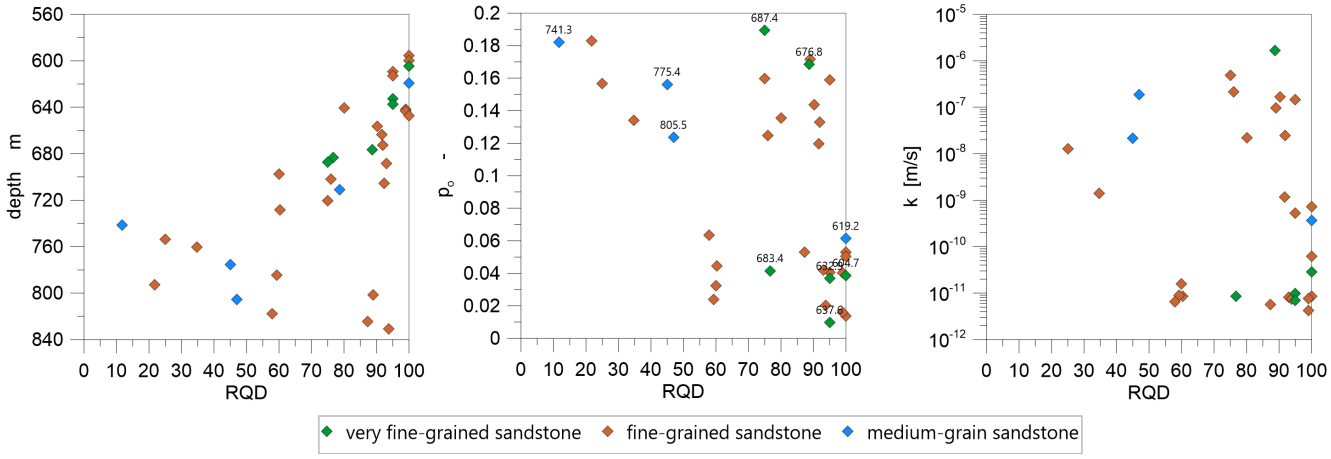

Figure 16. RQD vs. depth, p_o and k in the sandstone.

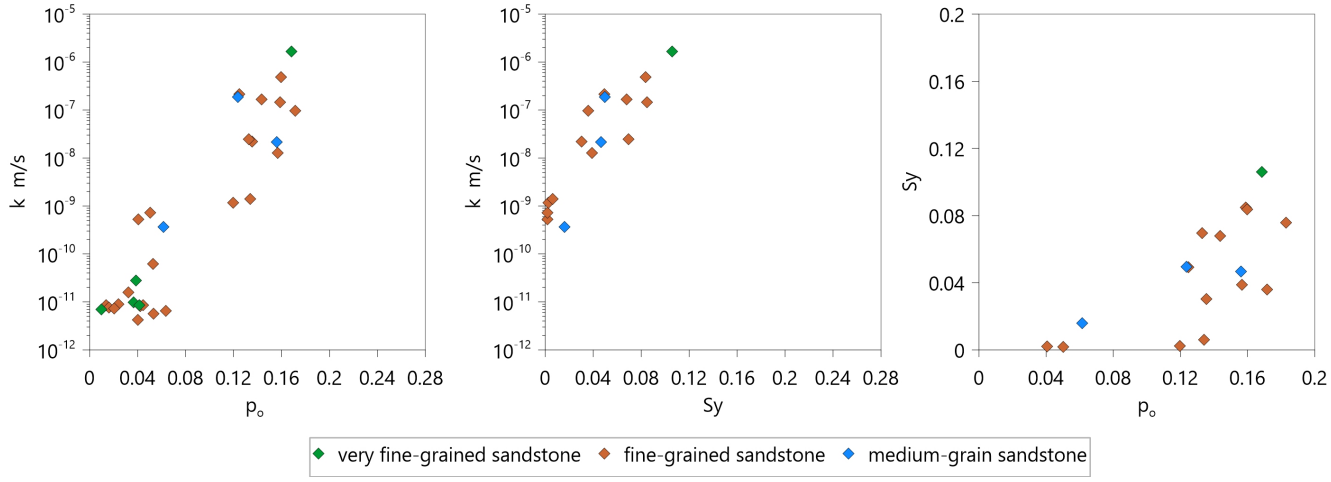

Figure 17. k vs. p_o and S_y, p_o vs. S_y.

4. Discussion

The middle and lower Bunter sandstone horizon is characterized by high horizontal and vertical variability in terms of water flow. It is formed in fine- and medium-grained, medium-bedded sandstone, locally brittle and multi-directionally fractured. Core recovery was observed in a wide range of 10–90%. Additionally, mudflow escapes were common while drilling this horizon.

RQD parameter analysis indicates the presence of a zone of mechanically strong, highly cemented sandstone and a zone of mechanically weak sandstone. In the weak zone, there are numerous clay inserts and delaminations. This results in privileged groundwater flow paths, reflected in mudflow escapes and large water inflows to the borehole. In the discussed borehole, such a zone occurs below a depth of 700 m. The negative correlation between RQD and p_o indicates that binder influences the level of permeable fractures. We observe lower interconnected porosity in rocks with higher strength and more binder. The second factor determining interconnected porosity is sandstone grain sorting. Samples with good sorting (medium-grained sandstone) have higher p_o values than samples with worse sorting (finer material fills the pore spaces).

The good correlation of p_o with S_y indicates a close relationship between these parameters, which is typical for sandstone where water fills the pore spaces. If a depression cone is formed, it is drained according to local pressure gradients and determines the long-term inflow to the mine workings.

One of the most important parameters determining the possibility of groundwater flow is hydraulic conductivity (k). The studied samples show three subgroups of results

with different water filtration properties, which depend mainly on pore formation and connections between them. Low values of *k* are found in local weak zones of the rock mass, which may indicate admixtures of clay minerals that fill the pore space and restrict water flow. Analysis of the results from the laboratory measurements shows that we obtain much lower *k* values in these studies than in the pumping tests. Only the six highest *k* values from laboratory measurements were similar to the *k* result from the pumping test. It means that direct adopting the results of laboratory measurements to calculate groundwater inflow gives the underestimated ability of rock mass drainage.

Information from archival hydrogeologic documentation was collected to evaluate the results on a regional scale. These are data from pumping tests performed in the middle and lower Bunter sandstone horizon since the 1970s. One hundred verified field tests were used to create a probability distribution plot of *k*. Results show hydraulic conductivity calculated from the single well (borehole) pumping tests ranging from 2.30×10^{-8} m/s to 2.60×10^{-6} m/s (Figure 18, blue points), average 6.48×10^{-7} m/s. The results obtained during the pumping tests classify the rocks into semi-permeable [51] or low-permeable rocks [52].

The *k*-values estimated based on current laboratory tests and pumping well W-1 are plotted on this graph for comparison to archival results from pumping tests. The W-1 pumping test results indicate that the rocks are low permeable and included in the regional values' upper zone. The laboratory results are shifted towards lower values and indicate that very low and low permeability rocks dominate. Such laboratory and pumping *k* values distribution suggest that the inflow to the mine will have two components (short-term and long-term), as described below, that are related to the scale of water-bearing voids.

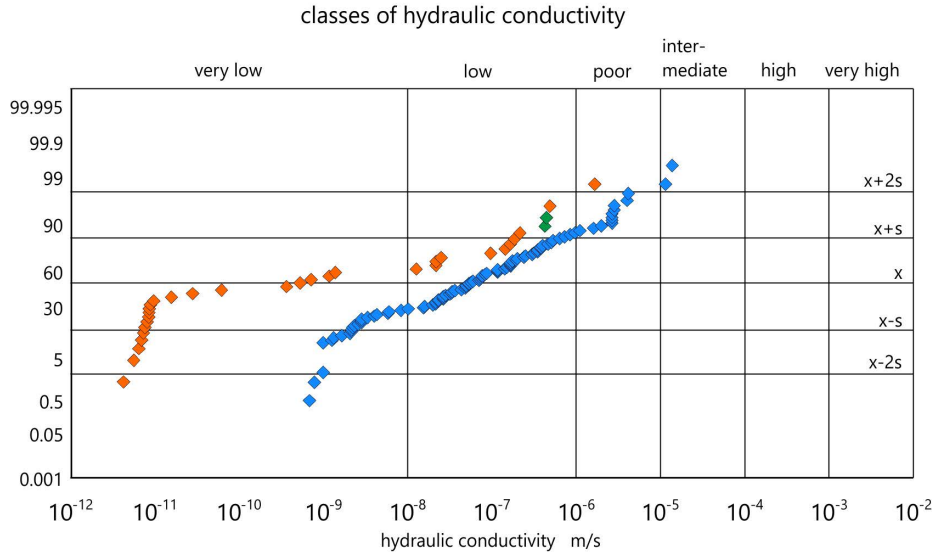

Figure 18. Values of the hydraulic conductivity of the middle and lower Bunter sandstone horizons determined from a single well pumping test (blue) ([53]), W-1 well-pumping test (green), and laboratory tests (orange) within the current study. x ± s: mean ± standard deviation, x ± 2s: mean ± 2 times standard deviation. Classification according to the *Hydrogeological Dictionary* [45].

The tested volume of the aquifer or sample strongly influences the obtained results, as was also proved by studies conducted in various laboratories (e.g., [18,54,55]). Different k values are obtained under laboratory conditions and during field measurements for the same sampled lithological interval (Figure 19). However, hydraulic conductivity increases with the scale of the tested pore-fissure rock mass (Figure 19). The same rule was observed in a described case; k measured in a laboratory is tenfold lower than in the pumping test in the well W-1. Moreover, such a distribution of results indicates that the pumping test shows the drainage ability of large rock intervals and gives information on water stored

in privileged regional structures (tectonic zones, rock faults, connected voids, etc.). These structures will be drained at first during the opening of the deposit and will provide a large and fast inflow (short-term component). They will also be responsible for the inflow to the shaft during the sinking operation. The laboratory measurements indicate values typical for the local rock matrix that will determine the inflow conditions to the mine long after the drained privileged zones. It will shape the long-term and smaller-intensity inflow.

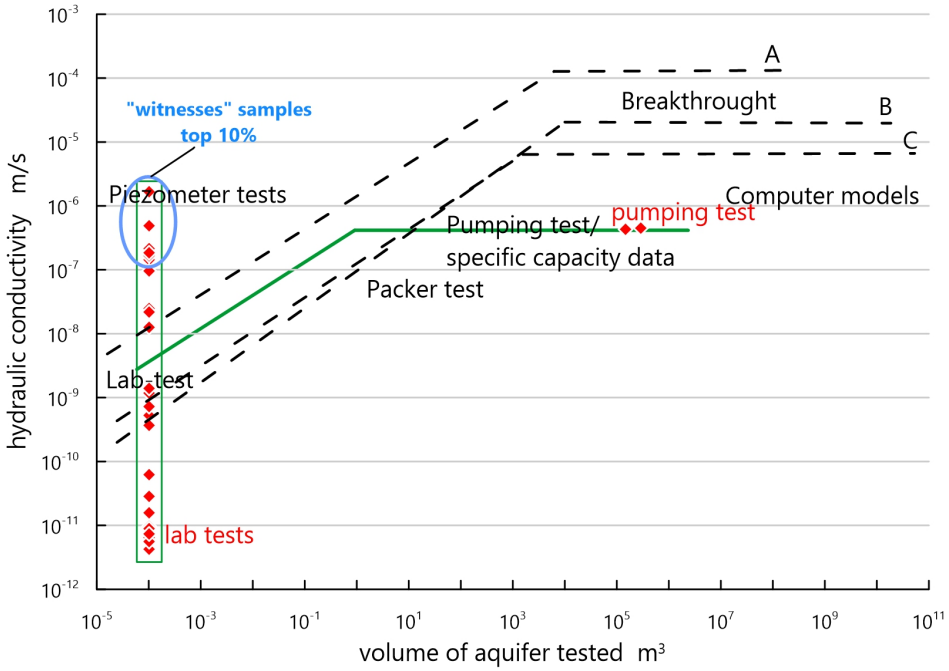

Figure 19. Dependence of the hydraulic conductivity on the volume of the tested rock mass. Green line: Fore-Sudetic Monocline Triassic sandstone, Black dashed lines: carbonate series rocks A: Thiensville Formation, B: Mayville carbonate rocks, C: Romeo carbonate rocks [56] after [55].

While discussing scale influence on hydraulic conductivity, we should also consider the thickness of the studied aquifer, which plays an important role in shaping the inflow to the sinking shaft. Parametrically it is defined by water transmissivity index T [m^2/s], which is a function of the properties of the liquid, the aquifer, and the thickness of the porous media [57]. In the study area, the average thickness of the middle and lower Bunter sandstone water-bearing formations reaches about 450 m. Consequently, the water transmissivity T index determined from the averaged pumping test results ranges from 1.82×10^{-4} m^2/s to 2.00×10^{-4} m^2/s (15.72–17.28 m^2/d). Therefore, according to the VI step classification proposed by J. Krásný (1993) [58], we classify the hydraulic transmissivity of the middle and lower Bunter sandstone horizon as class III: intermediate water transmissivity.

5. Conclusions

The process of sinking a mine shaft is a technologically challenging operation, especially in complex geological conditions. As described in the article, the Fore-Sudetic Monocline is precisely one of the areas with challenging geology. In order to reach a copper ore deposit at present, it is necessary to mine more than 1200 m deep and to pass through many aquifers. To date, the commonly used methodology for predicting inflows to the shaft has relatively often proved inaccurate and unreliable due to unrepresentative values of the hydraulic conductivity obtained from simple or inadequate estimates. An accurate assessment of the hydrogeological conditions and estimating the expected inflows to the sunken shaft determines its construction technology and influences the crew's safety and investment.

Our work and other scientific articles prove it [10,56,59] that to obtain the most realistic inflow predictions, it is necessary to rely on hydrogeological parameters from long-term pumping tests at nodes. However, such surveys for shafts deeper than 1000 m are extremely costly and time-consuming, and hence there is often great resistance to their use. Performing a long-duration pumping test also delays the mining works associated with the shaft excavation, which is also an unfavorable factor for performing this testing. New to our work were hydraulic conductivity measurements obtained from laboratory tests for samples obtained from drill cores. These types of samples are easy to collect in the course of drilling works related to the rock mass's reconnaissance and the subsequent shaft excavation. It is obvious that these samples characterize hydrogeological parameters on a point scale. Still, their sufficiently large population makes it possible to estimate a representative value of the hydraulic conductivity of the whole rock mass.

Our research showed that lab tests underestimate hydraulic parameters of the pore-fissure Triassic sandstone (mean hydraulic conductivity $k = 9.79 \times 10^{-8}$ m/s) tenfold more than long-term pumping tests (mean $k = 4.45 \times 10^{-7}$ m/s). This situation is consistent with cases known from the literature of the influence of the test scale on the values of the hydraulic conductivity in porous and pore-fissure aquifers with low rock matrix porosity. In our study for the Triassic sandstone, we found that this underestimation, i.e., the ratio of the hydraulic conductivity value obtained from the pumping test to the mean value of this parameter from the laboratory method, is relatively small and amounts to less than an order of magnitude ("underestimation" ratio = 4.54). The results published in the literature for fractured karst rocks show a difference in the results from laboratory tests and pumping tests of up to several orders of magnitude.

Individual laboratory samples cannot indicate the representative value of hydraulic conductivity, as it depends strongly on the research scale. Hydraulic conductivity typically increases with the test scale and then approaches an asymptote (Figure 19). Only if the tests cover the rock mass volume of at least 10,000–100,000 m^3 is it possible to obtain representative values of the hydrogeological parameters, including hydraulic conductivity. In such a volume, it is highly probable to capture most of the privileged zones affecting the groundwater flow conditions, e.g., those associated with higher porosity or characterized by a higher density of cracks.

For porous and pore-fissure rocks, such as the studied sandstone, collecting a large population of samples with the most diverse porosity makes it possible to find "witnesses" samples with parameter values close to a representative. This situation does not occur in the case of published studies of carbonate rocks where the permeability is related only to cracks and not to the porosity of the matrix (e.g., [18,39,54]. Based on our research, it can be concluded that the group of these "witness samples", for which the values of the hydraulic conductivity correspond to the representative value from the pumping test, comprises 10% of all core samples tested in the laboratory. With this in mind, we recommend using the highest values of hydrogeological parameters from laboratory tests based on the worst-case scenario. Therefore, it is possible to forecast inflows to the shafts reliably. This methodology is recommended only for rocks of porous and pore-fissure character. We recommend continuing research in this area to confirm whether the relationship found is valid only for the studied Triassic sandstone from the area of the Fore-Sudetic Monocline or also for all sandstone types from other locations.

The main conclusion of practical importance arising from our study is the confirmation of the relatively very low values of the hydraulic conductivity for Triassic sandstone from the area of the Fore-Sudetic Monocline. This is confirmed by results obtained by two methods at different scales, not only from drill core samples but from long-term and much more representative pumping tests.

The very low values of the hydraulic conductivity of the Triassic sandstone mean that, consequently, the expected inflows to the deep shaft will also be relatively small and technically feasible to drain using pumps. We, therefore, recommend considering the use of direct dewatering techniques for the rock mass without the need to freeze the ground,

which for deeper parts of the rock mass above 1 km is costly and technically difficult due to the high temperature of the rock and the presence of highly saline groundwater (brines).

Author Contributions: Conceptualization, M.P., M.W.-K., K.C. and M.C.; methodology, M.P., M.W.-K., K.C. and M.C.; software, M.P.; validation, M.P. and M.C.; formal analysis, M.P. and K.C.; investigation, M.P. and K.C.; resources, M.P., M.W.-K. and K.C.; data curation, M.W.-K. and K.C.; writing—original draft preparation, M.P., M.W.-K. and K.C.; writing—review and editing, M.W.-K. and K.C.; visualization, M.P. and K.C.; supervision, M.W.-K. and M.C.; project administration, M.W.-K.; funding acquisition, M.W.-K. and K.C. All authors have read and agreed to the published version of the manuscript.

Funding: The research work was partially funded with the grant co-financed by NCBiR and KGHM Polska Miedź S.A., entitled "IMore—Innovative methods of accessing deep deposits" (No. CuBR/I/1/NCBiR/2014) under the CuBR program and Wrocław University of Science and Technology research fund from the Polish Ministry of Education and Science granted for 2023.

Conflicts of Interest: The authors declare no conflict of interest.

References

1. Kalisz, M.; Niedbał, M. Wpływ odwadniania utworów triasowych w trakcie głębienia szybu R–XI na warunki hydrodynamiczne i powierzchniowe w północnej części OG "Rudna". *Mater. Symp. Nauk. Probl. Hydrogeol. Górnictwa Rud Miedzi* **2004**, 148–160.
2. Chudy, K.; Worsa-Kozak, M.; Pikuła, M. Rozwój metod rozpoznania warunków hydrogeologicznych na potrzeby wykonywania pionowych wyrobisk udostępniających złoże-przykład LGOM [Evolution of methods for hydrogeological condition recognition for the need of shaft sinking: An example from the Legnica-Glogow Copper District]. *Przegląd Geol.* **2017**, *65*, 1035–1043. Available online: https://geojournals.pgi.gov.pl/pg/article/view/27216/18934 (accessed on 2 December 2022).
3. Bocheńska, T.; Leśniak, L.; Tomaszewski, J. Związek między zawodnieniem wyrobisk górniczych a cechami litologicznymi i strukturalnymi górotworu. *Przegląd Geol.* **1971**, *19*, 278–284. Available online: https://geojournals.pgi.gov.pl/pg/article/view/23497/16362 (accessed on 2 December 2022).
4. Bocheńska, T.; Fiszer, J.; Kalisz, M. Weryfikacja prognoz dopływów do kopalń w Legnicko—Głogowskim Obszarze Miedzionośnymna podstawie badań modelowych. *Współczesne Probl. Hydrogeol.* **1995**, *VII*, 39–46.
5. Bocheńska, T.; Fiszer, J.; Kalisz, M. Prediction of groundwater inflow into copper mines of the Lubin Glogow Copper District. *Environ. Geol.* **2000**, *39*, 587–594. [CrossRef]
6. Bocheńska, T.; Bieniewski, J. Dopływ wód podziemnych do kopalni rudy miedzi na monoklinie przedsudeckiej. *Geol. Sudet.* **1978**, *XIII*, 133–141. [CrossRef]
7. Bocheńska, T.; Borysow, M. Zastosowanie metod modelowania elektrohydrodynamicznego do prognozy zawodnienia szybów [Application of electrohydrodynamic modeling methods to predict shaft inflows]. *Tech. Posz. Geol. Geosyn. Geoter.* **1982**, *3*, 35–38.
8. Sawicki, J.; Derkowska-Sitarz, M. Methods of definition of parts of water inflow from groundwater storage and groundwater renewable resources in total water inflow to mines. *Min. Sci.* **2006**, *8*, 167.
9. Pikuła, M.; Worsa-Kozak, M.; Chudy, K.; Kaczorek, K.; Szymański, A. Zastosowanie zmodyfikowanej metody analogii hydrogeologicznej z wykorzystaniem GIS w prognozowaniu dopływu wód do podziemnych wyrobisk górniczych [Application of modified hydrogeological analogy method using GIS in forecasting water inflow to underground mine workings]. *Górnictwo Odkryw.* **2018**, *2*, 67–75.
10. Zuber, A.; Motyka, J. Matrix porosity as the most important parameter of fissured rocks for solute transport at large scales. *J. Hydrol.* **1994**, *158*, 19–46. [CrossRef]
11. Gurwin, J.; Staśko, S.; Wcisło, M. Dokładność odwzorowa nia wielowarstwowych systemów hydrogeologicznych na szczegółowych modelach numerycznych—Analiza dla obszaru LGOM [Hydrogeological regional model as a permanent tool in solving various-scale tasks—Experience from the Legnica–Glogow Copper Region (LGOM)]. *Modele Mat. Hydrogeol.* **2014**, *471*, 45–50.
12. Staśko, S.; Gurwin, J.; Wcisło, M.; Modelska, M.; Kryza, H.; Kryza, J.; Olichwer, T.; Buczyński, S.; Tarka, R.; Wąsik, M.; et al. Model koncepcyjny systemu hydrogeologicznego obszaru oddziaływania Lubińsko-Głogowskiego Obszaru Miedzionośnego (LGOM) [Conceptual model of hydrogeological system of Lubin-Głogów Ore District impact area]. *Biul. Państwowego Inst. Geol.* **2012**, *451*, 203–210.
13. Lloyd, J.W.; Edwards, M.G. Estimation of groundwater inflow to an underground mining operation. *Int. J. Mine Water* **1988**, *7*, 25–47. [CrossRef]
14. Rapantova, N.; Grmela, A.; Vojtek, D.; Halir, J.; Michalek, B. Ground Water Flow Modelling Applications in Mining Hydrogeology. *Mine Water Environ.* **2007**, *26*, 264–270. [CrossRef]
15. d'Obyrn, K.; Kamiński, P.; Motyka, J. Influence of Hydrogeological Investigation's Accuracy on Technology of Shaft Sinking and Design of Shaft Lining—Case Study from Southern Poland. *Energies* **2021**, *14*, 2050. [CrossRef]

16. Beattie, D.; Bashir, R.; Hatley, J. Impact of Geotechnical and Hydrogeological Parameters upon Shaft Sinking Performance in the Athabasca Basin Canada. In *Mine Water and the Environment;* Rapantova, N., Hrkal, Z., Eds.; VSB—Technical University of Ostrava: Ostrava, Czech Republic, 2008; pp. 3–6. Available online: https://www.imwa.info/docs/imwa_2008/IMWA2008_141_Beattie.pdf (accessed on 2 December 2022).
17. Tiedeman, C.R.; Hill, M.C.; D'Agnese, F.A.; Faunt, C.C. Methods for using groundwater model predictions to guide hydrogeologic data collection, with application to the Death Valley regional groundwater flow system. *Water Resour. Res.* **2003**, *39*, 1010. [CrossRef]
18. Pinto da Cunha, A. *Scale Effects in Rock Masses 93*; CRC Press: Boca Raton, FL, USA, 1993. [CrossRef]
19. Nastev, M.; Savard, M.M.; Lapcevic, P.; Lefebvre, R.; Martel, R. Hydraulic properties and scale effects investigation in regional rock aquifers, south-western Quebec, Canada. *Hydrogeol. J.* **2004**, *12*, 257–269. [CrossRef]
20. Dausse, A.; Leonardi, V.; Jourde, H. Hydraulic characterization and identification of flow-bearing structures based on multi-scale investigations applied to the Lez karst aquifer. *J. Hydrol. Reg. Stud.* **2019**, *26*, 100627. [CrossRef]
21. Sánchez-Vila, X.; Carrera, J.; Girardi, J.P. Scale effects in transmissivity. *J. Hydrol.* **1996**, *183*, 1–22. [CrossRef]
22. Le Borgne, T.; Bour, O.; Paillet, F.; Caudal, J.P. Assessment of preferential flow path connectivity and hydraulic properties at single-borehole and cross-borehole scales in a fractured aquifer. *J. Hydrol.* **2006**, *328*, 347–359. [CrossRef]
23. Godoy, V.A.; Zuquette, L.V.; Gómez-Hernández, J.J. Scale effect on hydraulic conductivity and solute transport: Small and large-scale laboratory experiments and field experiments. *Eng. Geol.* **2018**, *243*, 196–205. [CrossRef]
24. Ghanbarian, B. Estimating the scale dependence of permeability at pore and core scales: Incorporating effects of porosity and finite size. *Adv. Water Resour.* **2022**, *161*, 104123. [CrossRef]
25. Konstantynowicz, E. *Monografia Przemysłu Miedziowego w Polsce*; Wydawnictwa Geologiczne: Warszawa, Poland, 1971.
26. Kiersnowski, H.; Petecki, Z. Budowa geologiczna podcechsztyńskiego podłoża Legnicko-Głogowskiego Okręgu Miedziowego (LGOM) i jego otoczenia: spojrzenie krytyczne [Geology of the Zechstein basement of the Legnica-Głogów Copper] District (LGOM) and its surroundings: A critical overview. *Biul. Państwowego Inst. Geol.* **2017**, *468*, 175–198. Available online: http://yadda.icm.edu.pl/baztech/element/bwmeta1.element.baztech-292ac488-6bc9-4b25-a9fc-dba25f56a442 (accessed on 2 December 2022).
27. Kaczmarek, W.; Kaczmarek, W.; Twardowski, M.; Wasilewska-Błaszczyk, M. Praktyczne aspekty modelowania litologicznych typów rud w złożach cu-ag LGOM(Legnicko-Głogowskiego Okręgu Miedziowego). *Biul. Państwowego Inst. Geol.* **2016**, *468*, 209–226.
28. Wodzicki, A.; Piestrzyński, A. An ore genetic model for the Lubin—Sieroszowice mining district, Poland. *Miner. Depos.* **1994**, *29*, 30–43. [CrossRef]
29. Piestrzyński, A.; Banaszak, A.; Zaleska-Kuczmierczyk, M. *Monografia KGHM Polska Miedź S.A.*, 2nd ed.; KGHM Polska Miedz S.A.: Lubin, Poland, 2007; p. 1086.
30. Dąbrowski, S.; Przybyłek, J. *Metodyka Próbnych Pompowań w Dokumentowaniu Zasobów wód Podziemnych. Poradnik Metodyczny*; Ministerstwo Środowiska: Warszawa, Poland, 2005; p. 292.
31. Gonet, A.; Macuda, J.; Zawisza, L.; Duda, J.; Porwis, J. *Instrukcja Obsługi Wierceń Hydrogeologicznych [Hydrogeological Drilling Operations Manual]*; Wydawnictwa AGH: Kraków, Poland, 2011; p. 134.
32. Agarwal, R.G. A New Method To Account For Producing Time Effects When Drawdown Type Curves Are Used To Analyze Pressure Buildup And Other Test Data. In Proceedings of the SPE Annual Technical Conference and Exhibition, Dallas, TX, USA, 21–24 September 1980. [CrossRef]
33. Agarwal, R.G.; Al-Hussainy, R.; Ramey, H. An Investigation of Wellbore Storage and Skin Effect in Unsteady Liquid Flow: I. Analytical Treatment. *Soc. Pet. Eng. J.* **1970**, *10*, 279–290. [CrossRef]
34. Röhrich, T. *AquiferTest v.4.2 User's Manual*; Schlumberger Water Services: Waterloo, ON, Canada, 2005.
35. Theis, C.V. The relation between the lowering of the Piezometric surface and the rate and duration of discharge of a well using ground-water storage. *Trans. Am. Geophys. Union* **1935**, *16*, 519. [CrossRef]
36. Mays, L.W.; Todd, D.K. *Groundwater Hydrology*; Wiley & Sons: Hoboken, NJ, USA, 2004; p. 656.
37. Deere, D.; Hendron, A.; Patton, F.; Cording, E. Design of Surface and Near Surface Construction in Rock. In Proceedings of the 8th U.S. Symposium on Rock Mechanics (USRMS), Minneapolis, MN, USA, 15–17 September 1966; pp. 237–302.
38. Schön, J. Geomechanical Properties. In *Handbook of Petroleum Exploration and Production*; Elsevier: Amsterdam, The Netherlands, 2011; Volume 8, pp, 245–271. [CrossRef]
39. Carmichael, R.S. *Practical Handbook of Physical Properties of Rocks and Minerals (1988)*; CRC Press: Boca Raton, FL, USA, 2017. [CrossRef]
40. Borczak, S.; Motyka, J.; Pulido-Bosch, A. The hydrogeological properties of the matrix of the chalk in the Lublin coal basin (southeast Poland). *Hydrol. Sci. J.* **1990**, *35*, 523–534. [CrossRef]
41. James, O.D.; Lee, P.C.Y. Flow in fractured porous media. *Water Resour. Res.* **1977**, *13*, 558–566. [CrossRef]
42. Motyka, J. A conceptual model of hydraulic networks in carbonate rocks, illustrated by examples from Poland. *Hydrogeol. J.* **1998**, *6*, 469–482. [CrossRef]
43. Motyka, J.; Pulido-Bosch, A.; Borczak, S.; Gisbert, J. Matrix hydrogeological properties of Devonian carbonate rocks of Olkusz (Southern Poland). *J. Hydrol.* **1998**, *211*, 140–150. [CrossRef]

44. Motyka, J.; Pulido-Bosch, A. Karstic phenomena in calcareous-dolomitic rocks and their influence over the inrushes of water in lead-zinc mines in Olkusz region (South of Poland). *Int. J. Mine Water* **1985**, *4*, 1–11. [CrossRef]
45. Dowgiałło, J.; Kleczkowski, A.; Macioszczyk, T.; Różkowski, A. *Słownik Hydrogeologiczny [Hydrogeological Dictionary]*; Państw. Inst. Geol.: Warszawa, Poland, 2002; p. 461.
46. Agarwal, V.C. *Groundwater Hydrology*; PHI Learning Pvt. Ltd.: Delhi, India, 2012; p. 372.
47. Motyka, J.; Szczepańska, J.; Witczak, S. Zastosowanie wirówki do badania współczynnika odsączalności i dynamiki oddawania wody przez skałę. *Tech. Poszuk.* **1971**, *37*, 38–43.
48. Prill, R.C.; Johnson, A.I.; Morris, D.A. *Specific Yield—Laboratory Experiments Showing the Effect of Time on Column Drainage*; U.S. Geological Survey: Reston, VA, USA, 1965; p. 55.
49. Motyka, J.; Postawa, A. Influence of contaminated Vistula River water on the groundwater entering the Zakrzowek limestone quarry, Cracow region, Poland. *Environ. Geol.* **2000**, *39*, 398–404. [CrossRef]
50. Duliński, W. Aparat do badania przepuszczalnosci z uszczelnieniem pneumatycznym. *Wiadomości Naft.* **1965**, *7*, 117–118.
51. Pazdro, Z. *Hydrogeologia Ogólna [Hydrogeology]*; Wydaw. Geologiczne: Warszawa, Poland, 1983; p. 575.
52. Head, K.; Epps, R. Manual of Soil Laboratory Testing—Volume 2: Permeability, Shear Strength and Compressibility Tests. *Q. J. Eng. Geol. Hydrogeol.* **2014**, *47*, 191–191. [CrossRef]
53. Bezkorowajny, A.; Stochel, B.; Chudy, K.; Worsa-Kozak, M.; Cygan, S.; Janicki, D.; Kalisz, M.; Konsencjusz, D.; Merta, A.; Szumilas, P. Dokumentacja Hydrogeologiczna Określająca Warunki Hydrogeologiczne w Związku z Zamierzonym Wykonywaniem Odwodnień w celu Wydobywania rud Miedzi ze złoża Rudna. 2013, *unpublished*.
54. Zhan, S.S.; Wang, T.T.; Huang, T.H. Variations of hydraulic conductivity of fracture sets and fractured rock mass with test scale: Case study at Heshe well site in Central Taiwan. *Eng. Geol.* **2016**, *206*, 94–106. [CrossRef]
55. Schulze-Makuch, D.; Cherkauer, D.S. Variations in hydraulic conductivity with scale of measurement during aquifer tests in heterogeneous, porous carbonate rocks. *Hydrogeol. J.* **1998**, *6*, 204–215. [CrossRef]
56. Drożdżak, R.; Twardowski, K. Wpływ efektu skali na wyniki badań przepuszczalności porowatych ośrodków gruntowo-skalnych [Influence of scale effect on the results of permeability tests on rock-ground porous media]. *Wiert. Naft. Gaz* **2009**, *26*, 599–611.
57. Şen, Z. Chapter 2—Basic Porous Medium Concepts. In *Practical and Applied Hydrogeology*; Şen, Z., Ed.; Elsevier: Oxford, UK, 2015; pp. 43–97. [CrossRef]
58. Krasny, J. Classification of Transmissivity Magnitude and Variation. *Ground Water* **1993**, *31*, 230–236. [CrossRef]
59. Ziemianin, K.; Jędrzejowska-Tyczkowska, H. Efekt skali w interpretacji geologicznej danych geofizycznych i analiz laboratoryjnych—Wprowadzenie do tematyki oraz przykłady obliczeń na danych modelowych [Scale effect in geological interpretation of geophysical and laboratory data—Introduction to the topic and model data calculations examples]. *Nafta-Gaz* **2013**, *69*, 719–734.